High-performance SOD mimetic enzyme Au@Ce for arresting cell cycle and proliferation of acute myeloid leukemia

Yuxiang Sun [a,1], Xin Liu [a,1], Lei Wang [b,1], Li Xu [c], Kunliang Liu [d], Lei Xu [b], Fangfang Shi [e], Yu Zhang [a], Ning Gu [a,**], Fei Xiong [a,*]

[a] State Key Laboratory of Bioelectronics, Jiangsu Key Laboratory for Biomaterials and Devices, School of Biological Science and Medical Engineering & Collaborative Innovation Center of Suzhou Nano-Science and Technology, Southeast University, Nanjing, 210096, PR China
[b] Department of Gastroenterology, Nanjing Drum Tower Hospital, Affiliated Hospital of Nanjing University Medical School, Nanjing University, Nanjing, PR China
[c] Jiangsu Key Laboratory of Molecular Medicine, Medical School of Nanjing University, Nanjing, 210093, PR China
[d] Department of Research and Development, Jinan Guoke Medical Technology Development Co., Ltd., Address: No. 1, Gangxing 3rd Road, High-tech Industrial Development Zone, Jinan City, Shandong Province, 250013, PR China
[e] Department of Oncology, Zhongda Hospital, Southeast University, Nanjing 210009, China

ARTICLE INFO

ABSTRACT

SOD-like activity of CeO$_2$ nanoparticles (Ce NPs) is driven by Ce^{3+}/Ce^{4+}, high oxidative stress can oxidize Ce^{3+} to reduce the ratio of Ce^{3+}/Ce^{4+}, inactivating the SOD activity of Ce NPs. Herein, we found Au@Ce NPs, assembled by Au NPs and Ce NPs, exhibited high-performance of SOD mimetic enzyme activity even upon the oxidation of H$_2$O$_2$. Ce NPs supported by nano-Au can acquire the electrons from Au NPs through the enhanced localized surface plasmon resonance (LSPR), maintaining the stability of Ce^{3+}/Ce^{4+} and SOD-like activity. Meanwhile, Au@Ce NPs retained the peroxidase function and catalase function. As a result, Au@Ce NPs effectively scavenged O$_2$•- and the derived ROS in AML cells, which are the important signaling source that drives AML cell proliferation and accelerates cell cycle progression. When HL-60 cells were treated by Au@Ce NPs, the removal of endogenous ROS signal significantly arrested cell cycle at G1 phase and suppressed the cell proliferation by blocking the mitogen-activated protein kinases (MAPKs) signaling and the Akt/Cyclin D1 cell cycle signaling. Importantly, this treatment strategy showed therapeutic effect for subcutaneous transplantation of AML model as well as a satisfactory result in diminishing the leukocyte infiltration of liver and spleen particularly. Thus, assembled Au@Ce NPs show the high-performance SOD-like activity, promising the potential in treating AML and regulating abnormal ROS in other diseases safely and efficiently.

1. Introduction

Acute myeloid leukemia (AML) is an aggressive hematopoietic malignancy, characterized by proliferation of blast cells and destruction of hematopoietic function in patients [1]. AML patients will suffer from relapse with a high probability after chemotherapy or stem cell transplantation [2,3]. Thus, novel strategies are urgently required for AML patients. Previous evidences have reported that AML blast cells has a distinct feature of higher oxidative stress, especially for oxygen radical with a higher level in malignant cells than that in normal leukocytes [4,5]. The treatment strategy targeted to intracellular reactive oxygen species (ROS) as the intervention target showed potential application prospects [6,7].

ROS derived by mitochondrial electron transport chain (ETC) or nicotin-amide adenine dinucleotide phosphate (NADPH) oxidases (NOXs) plays an important role in hematopoiesis and maintaining the proliferation of leukemia cells [8–11]. Elevated homeostasis ROS functioned as the secondary messenger to activate mitogen-activated protein kinases (MAPKs) signaling [9,12,13], mitochondrial cascade signaling and cell cycle signaling [14], leading to the malignant proliferation and aggressiveness of AML [15]. A number of independent studies have shown that ROS-activated p38MAPK induced the loss of self-renewal of

hematopoietic stem cells, while eliminating ROS can inactivate p38MAPK to further inhibit the proliferation of AML cells [11]. In addition, ROS-mediated Akt/GSK-3/Cyclin cascade accelerated the process of cell cycle in many malignant proliferative cells including AML cells [16–18]. Therefore, some small molecular compounds that can scavenge free radicals exhibited the ability to arrest cell cycle and promote AML cell apoptosis [14,19,20].

Superoxide anion ($O_2\bullet$-), hydrogen peroxide (H_2O_2) and hydroxyl radical ($\bullet OH$) are the main oxygen radicals in cells. ETC-driven and NOXs-driven ROS in AML cells is mainly in the form of $O_2\bullet$- [21,22], which is then converted to H_2O_2 by superoxide dismutase (SOD), and H_2O_2 is further decomposed into O_2 and H_2O by catalase (CAT) [23]. In fact, $O_2\bullet$-→H_2O_2→O_2/H_2O conversion axis mediated by intracellular antioxidant enzymes is the key mechanism that determines the level of intracellular ROS. Thus, there are two strategies to block ROS signaling in AML cells, one is to use antioxidants to reduce ROS level directly, the other is to accelerate the conversion axis of ROS by antioxidant enzymes [24]. However, the production of intracellular $O_2\bullet$- and H_2O_2 is continuous, the eliminated ROS can return to a high level again after the supplementary antioxidants failed to work. For the second strategy, ROS conversion axis are controlled by antioxidant enzymes (SOD and CAT), which are yet strictly controlled by the mechanism of corresponding DNA transcription. Additionally, natural SOD and CAT enzymes are both the macromolecular proteins, they are difficult to penetrate cell membrane and easy to cause alloantigen reaction. Importantly, the half-life of natural SOD in human blood is so short that it is hard to deliver them to the cancer lesions [25]. That means a great challenge to maintain high level of antioxidant enzymes in vivo.

Recently, artificial enzymes or nanozymes with SOD and CAT activity provided the potential to meddle in intracellular ROS conversion axis, and some reports have achieved ideal results for AML treatment by nanozymes [6,24]. Ceria nanoparticles (Ce NPs) exhibited excellent SOD-like and CAT-like activity and its SOD activity was reported higher than the nature SOD enzyme [24,26]. Thus, Ce NPs was widely used as a free radical scavenger to reduce intracellular ROS. Self et al. first discovered the SOD and CAT activity of Ce NPs and revealed that the activity of mimetic enzymes was dependent on Ce^{3+}/Ce^{4+} ratios [26–28]. Ce NPs with higher Ce^{3+}/Ce^{4+} ratios will get higher SOD mimic activity. They put forward the catalytic mechanism of mimetic SOD as follows:

$$O_2^- + Ce^{4+} \rightarrow O_2 + Ce^{3+}$$

$$O_2^- + Ce^{3+} + 2H^+ \rightarrow H_2O_2 + Ce^{4+}$$
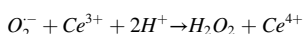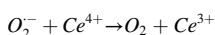
Accordingly, the SOD-like catalytic ability of Ce NPs suffered from the challenge of high oxidation, especially the high level of ROS in AML cells. Because H_2O_2 can oxidase the Ce^{3+} to Ce^{4+}, decreasing the Ce^{3+}/Ce^{4+} ratios as well as its SOD-like activity. Thus, we propose the strategy to increase the proportion of Ce^{3+} by assembling multi-electron donor to maintain the efficient SOD activity of Ce NPs even upon the high oxidation.

Gold nanoparticles (Au NPs) is also a kind of widely studied nanozymes that are of SOD-like and CAT-like activity, and there are a large number of free electrons on the surface [29]. In fact, these free electrons are easy to be induced. Some evidences indicated that the free electrons on Au NPs surface can be transferred to Ce NPs to enhance the redox ability between Ce^{3+} and Ce^{4+} after the assembly of Au NPs and Ce NPs [30,31]. Even, the enhanced localized surface plasmon resonance (LSPR) driven by photodynamic force on Au NPs surface can transfer free electrons to Ce NPs to conduct chemical reaction [32]. Some research have explored the multi-enzyme activity of assembled Au NPs and Ce NPs and demonstrated their excellent peroxidase (POD), CAT, and SOD-like activities, although these different enzyme-like activity was dependent on pH [33]. Interestingly, the enzymatic reactions are performed by the efficient electron transfers, especially hypothesized by

the electron transfer between the redox potentials of Au^+/Au and Ce^{3+}/Ce^{4+}.

In view of this, we assembled Au@Ce composite nanozyme with multi-enzyme activity of SOD and CAT. We found Ce NPs in the assembled Au@Ce NPs can obtain electrons from Au NPs to inhibit the oxidation of Ce^{3+} by the mechanism that H_2O_2 mediated enhanced LSPR on Au NPs, reversing the inhibition of Ceria SOD-like activity upon high oxidation condition (Scheme 1). Au@Ce NPs showed the more ideal SOD mimic enzyme function instead. Meanwhile, the relay between SOD and CAT from Au@Ce NPs promotes the scavenger to ROS free radicals in vitro and in vivo, which obviously arrested cell cycle of AML cells at G1 phase and induced apoptosis by down-regulating the expression of AKT/Cyclin D1 and MAPKs. In conclusion, assembled Au@Ce NPs can eliminate ROS through high-performance SOD activity and relay effect, showing great potential in the treatment of AML and oxidative stress disorders.

2. Results and discussion

2.1. Preparation and characterization

The preparation procedures of Au NPs, Ce NPs and Au@Ce NPs were shown in Fig. S1, all of them were stabilized with dextran (M_W: 40000). *Trans*-mission electron microscopy (TEM) revealed the appearance and size of Au NPs (Fig. 1A), Ce NPs (Fig. 1B) and Au@Ce NPs (Fig. 1C). Au nano-sphere and Au@Ce nano-sphere both have the similar Au core about 20 nm, but Au core in Au@Ce NPs are surrounded by Ce NPs, which was similar with colloidal solution of Ce NPs. EDS spectrum of Au@Ce NPs shows the existence of Au element and Ce element, their weight ratio of Au:Ce is about 1:2 (Fig. 1D). UV–Vis spectrum shows that Au@Ce NPs touch off the absorption at 530 nm assigned to Au NPs, as well as the near ultraviolet absorption at 290 nm assigned to Ce NPs (Fig. 1E). The absorbance at these two wavelengths is respectively proportional to the concentration of Au@Ce NPs, indicating a good homogeneity of assemblies (Fig. 1F and Fig. S2). Meanwhile, we observed that Au@Ce NPs solution can absorb UV-light to emit dark UV-light, especially emit ultraviolet spectrum at 380 nm wavelength upon the excitation by 310 nm UV-light (Fig. S3 and Fig. S4). In aqueous solution, hydrodynamic diameter of Au NPs and Au@Ce NPs are about 23 nm and 35 nm (Fig. 1G), and the stable hydrodynamic size distribution within 7 days demonstrates that Au@Ce NPs have good colloidal stability in aqueous solution (Fig. 1H). Meanwhile, all of the three kinds of NPs, Au@Ce NPs, Au NPs, Ce NPs, are near the neutral zeta-potential (Fig. S5). After lyophilized Ce NPs and Au@Ce NPs, their XRD pattern presents two sets of diffraction peaks (Fig. 1I). One is assigned to the CeO_2 phase and the other to the Au phase. These data prove that Au@Ce NPs are formed by the assembly of Au NPs and Ce NPs.

2.2. SOD-like, POD-like and CAT-like activity of Au@Ce NPs

As two nanozymes of multi-enzyme activities, Au NPs and Ce NPs both have been reported with the mimic enzyme functions like SOD, POD and CAT. Thus, their SOD, POD, and CAT enzyme activities were determined respectively by the classic methods of $O_2\bullet$-/NBT absorbance inhibition assay [34], HO$\bullet$/TMB absorbance increase assay [35], and H_2O_2/dissolved oxygen concentration change assay [36]. These tests revealed that Au NPs, Ce NPs, (Au + Ce) NPs mixture and Au@Ce NPs have enzymatic activity of SOD (Fig. 2A), POD (Fig. 2B) and CAT (Fig. 2C). Meanwhile, we evaluated the concentration dependence of the corresponding enzyme activities. Results showed that the multi-enzyme activities of Au@Ce NPs were all concentration-dependent (Fig. 2D–F). Of course, the SOD activity of other nanoparticles was all concentration-dependent (Fig. S6). Additionally, their POD enzyme activity requires a proper acidic environment because their POD-like activity almost disappears in weak acid conditions (pH higher than 5.0), especially for Au@Ce NPs (Fig. S7 and Fig. S8). That means it is difficult
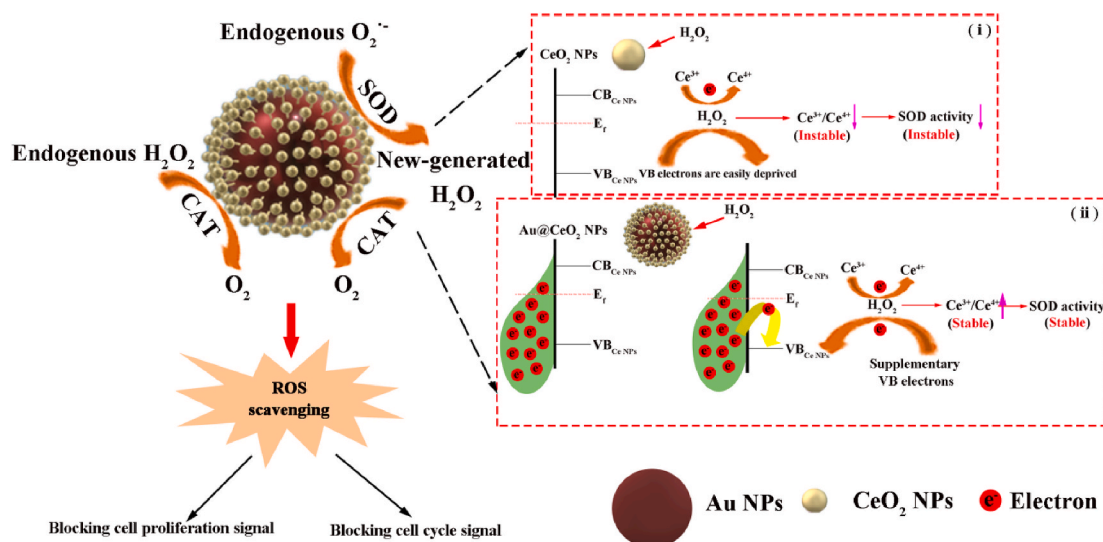
Scheme 1. Shows the mechanism that Au@Ce NPs interfere with ROS homeostasis and arrest cell cycle and proliferation through its high-performance SOD activity as well as the relay conversion of $O_2\bullet^- \to H_2O_2 \to O^2$. (i) Schematic of CeO_2 NPs SOD activity that was suppressed by the oxidation of H_2O_2. (ii) Schematic of Au@Ce NPs SOD activity that can maintain the stability against the oxidation of H_2O_2 according to the electron compensation effect from Au substrate.

for Au@Ce NPs to promote the conversion of $H_2O_2 \to HO\bullet$ upon regulating ROS in the body.

2.3. Au@Ce NPs can maintain the stability of Ce^{3+}/Ce^{4+} ratio

Among these tests, however, Au@Ce NPs exhibited more efficient SOD-like and POD-like activity compared to other groups at the same dose, but its CAT-like activity was worse than that of the Ce NPs group alone. According to reports, the enzymatic activity of Ce NPs is closely related to the ratio of Ce^{3+}/Ce^{4+} [26]. However, H_2O_2 can oxidase the Ce^{3+} to Ce^{4+}, the increase in the ratio of Ce^{4+} is more conducive to its CAT enzyme activity, on the contrary, which is detrimental to its SOD enzyme activity [37,38]. Therefore, we speculated, in H_2O_2-existed highly oxidizing environment, Ce NPs exhibited more efficient CAT but poor SOD enzyme activity.

According to the energy band theory of semiconductor crystal particles, the valence band energy level of CeO_2-x NPs is in full band. The oxidation of H_2O_2 can induce electron transition in the valence band of ceria crystals, thereby increasing the ratio of Ce^{4+} while leaving empty bands. After assembled the Ce NPs on Au NPs, free electrons on the surface of Au NPs can quickly fill the empty band of ceria crystals and promote the recovery of Ce^{3+} ratio, maintaining its SOD activity (Fig. 3A). Accordingly, we first explored the effect of H_2O_2 concentration on the LSPR of Au@Ce NPs by measuring the absorbance at 530 nm with the same concentration of Au@Ce NPs. As a result, the concentration-dependent increase of absorbance was observed after induction by different concentrations of H_2O_2, even sub-micromolar H_2O_2 can cause a sharp increase in absorbance at 530 nm (Fig. 3B). That means H_2O_2 can exacerbate the instability of free electrons on the surface of Au NPs and thus induced the enhancement of LSPR.

However, the instability of free electrons on the surface of Au NPs is beneficial to the SOD-like function of Ce NPs after assembled them, because the active electrons induced by H_2O_2 can timely reoccupy the empty band energy level in ceria crystal and maintain the stability of Ce^{3+}/Ce^{4+} by compensating electrons to reduce Ce^{4+} to Ce^{3+}. In order to prove that Au@Ce NPs can resist the oxidation of H_2O_2 and maintain the proportion of Ce^{3+}, we measured the change of Ce^{3+} ratio in Au@Ce NPs after treatment by different concentrations of H_2O_2. In the ultraviolet spectrum, ceria can cause two absorption peaks at 252 nm and 290 nm respectively assigned to Ce^{3+} and Ce^{4+} [37]. As shown in (Fig. 3C, D), H_2O_2-treated Au@Ce NPs shows the increase of Ce^{3+} ratio, contrary

to that is decrease in H_2O_2-treated Ce NPs. Moreover, H_2O_2-treated Ce NPs and Au@Ce NPs were analyzed by XPS to evaluate the ratio of Ce^{3+}/Ce^{4+} respectively. The results demonstrated again that H_2O_2 induced no obvious change of Ce^{3+}/Ce^{4+} ratio in Au@Ce NPs but a significant decrease of Ce^{3+}/Ce^{4+} ratio in Ce NPs by contrary (Fig. 3E and F). This suggests that Au@Ce NPs can protect the Ce^{3+} against the oxidation by H_2O_2 to preserve the stability of Ce^{3+}/Ce^{4+} ratio.

2.4. High-performance SOD activity of Au@Ce NPs

To this end, we explored the changes of SOD-like activity of Au@Ce NPs upon the oxidation by H_2O_2. As shown in Fig. 4A, with the increase of H_2O_2 in the reaction system, the inhibition of $O_2\bullet^-$ formation mediated by Ce NPs and (Au + Ce) NPs was significantly attenuated, where 0.025 M H_2O_2 mitigated the SOD-activity of Ce NPs and (Au + Ce) NPs by half, while they almost lost their ability to scavenging $O_2\bullet^-$ after oxidation of 0.05 M H_2O_2, reflecting in the inhibition rate dropped from 60 % to about 10 % (Fig. 4B). Correspondingly, SOD activity of Au@Ce NPs was less affected by H_2O_2, where 0.025 M H_2O_2 and 0.05 M H_2O_2 only diminished the 80 % inhibition ratio to 60 %. Importantly, even in the presence of 0.1 M H_2O_2, Au@Ce NPs remained 50 % inhibitory to $O_2\bullet^-$, suggesting the high-performance SOD-like activity of Au@Ce NPs (Fig. 4A and B). A similar phenomenon was also observed in ESR testing, that Ce NPs and Au@Ce NPs both exhibited the inhibition to $O_2\bullet^-$ ESR signal, but H_2O_2-treatd Ce NPs almost lose its inhibition function compared to the obvious inhibition by H_2O_2-treated Au@Ce NPs (Fig. 4C and D). Thus, Au@Ce NPs still has high-performance SOD activity against high oxidation conditions.

2.5. Scavenging intracellular ROS in HL-60 cells

Based on high-performance SOD activity of Au@Ce NPs, intracellular $O_2\bullet^-$ can be converted to H_2O_2 efficiently, while new-generated H_2O_2 and intracellular H_2O_2 were then decomposed to H_2O and O_2 with the assistance of CAT function from Au@Ce NPs. This relay conversion between ROS is conducive to scavenge intracellular ROS continuously. We first evaluated the effect of Au@Ce NPs on cell viability of HL-60, an acute myeloid leukemia cell line. As a result, cell viability was decreased in a concentration-dependent manner (Fig. 5A). Meanwhile, Au@Ce NPs has minimal negative effect on normal cells including vascular endo-thelial cells (HUVEC) and lymphocytes (GM14519) (Fig. S9). To prove
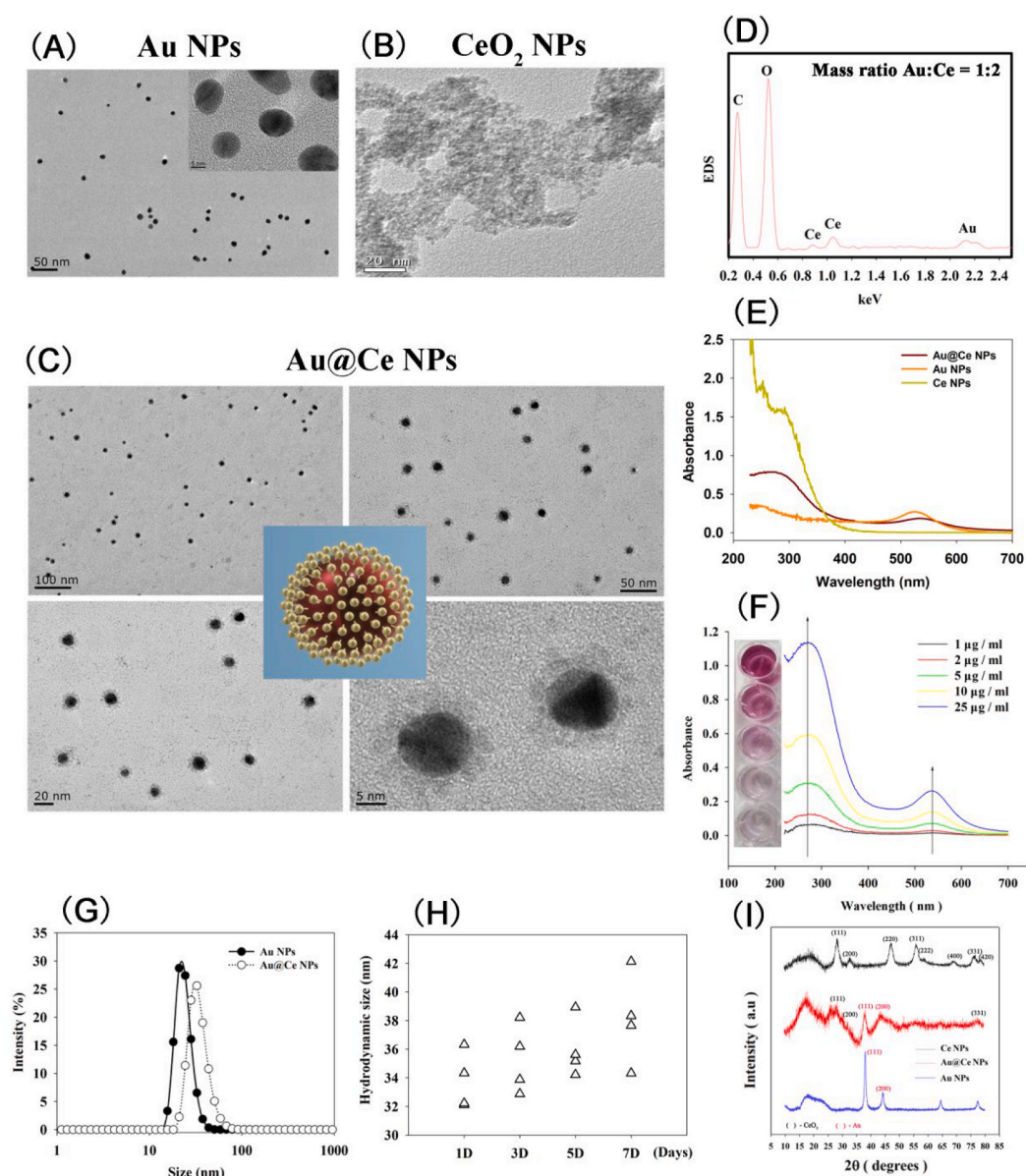
Fig. 1. Characterization of Au@Ce NPs. (A) TEM of Au@dextran NPs (Au NPs). (B) TEM of CeO$_2$@dextran NPs (Ce NPs). (C) TEM of Au@CeO$_2$@dextran NPs (Au@Ce NPs) and the schematic diagrams. (D) Energy Dispersive Spectrometer (EDS) of Au@Ce NPs. (E) UV–Vis spectra of Au NPs, Ce NPs and Au@Ce NPs. (F) UV–Vis spectra corresponding to different concentrations of Au@Ce NPs. (G) Hydrodynamic size distribution data of Au NPs and Au@Ce NPs. (H) Hydrodynamic size changes of Au@Ce NPs within 7 days in saline. (f) X-ray diffraction (XRD) of Ce NPs and Au@Ce NPs.

the excellent ROS scavenging ability of Au@Ce NPs, 5 μg/ml (Au + Ce) of Au@Ce NPs was used as the treatment concentration. And DHE fluorescent probe and DCFH fluorescent probe were used for the detection to O$_2\bullet$- and H$_2$O$_2$ respectively.

After treatment for 24 h, Au@Ce NPs induced the most significant decrease of DHE-labeled O$_2\bullet$- and DCFH-labeled H$_2$O$_2$, although alone Au, Ce and the mixed (Au + Ce) all exhibited the similar scavenging effect (Fig. 5B and C). Meanwhile, the changes of intracellular ROS were also detected by flow cytometry and fluorescence microscopy. And a similar result was demonstrated by that Au@Ce NPs inhibited intracellular O$_2\bullet$- more significantly than that of the mixed (Au + Ce) (Fig. 5D, F, H), but these two groups both showed the efficient ROS removal (Fig. 5E, G, I). Meanwhile, HPF-detected the level of HO$\bullet$ also showed the more conspicuous elimination to intracellular HO$\bullet$ in these cells after treatment by Au@Ce NPs (Fig. S10).

Additionally, we validated the results in two other cell lines THP-1 cells and WEHI-3 cells. THP-1 is the human monocytic leukemia cell and WEHI-3 is the acute myelomonocytic leukemia in mice. In THP-1 cells, after 24 h of treatment, Au@Ce NPs shows obvious inhibitory effect on cell viability (Fig. S11a), correspondingly, DHE-labeled O$_2\bullet$- (Fig. S11b) and DCFH-labeled ROS (Fig. S11c) were both reduced significantly. In WEHI-3 cells, we investigated the changes of cell viability, DHE-labeled O$_2\bullet$- and DCFH-labeled ROS. As results, Au@Ce NPs successfully induced the decrease of cell viability dependent on concentration (Fig. S12a). Correspondingly, intracellular fluorescence signal of DHE-labeled O$_2\bullet$- (Fig. S12b) and DCFH-labeled ROS (Fig. S12c) were both suppressed by Au@Ce NPs. These demonstrated the intervention effect of Au@Ce NPs on intracellular ROS and the proliferation in AML cells. Given that there are high levels of O$_2\bullet$- in AML cells [8,21,23], from this point of view, Au@Ce NPs may be specificity for AML.

2.6. Au@Ce NPs arrested cell cycle and proliferation in HL60 cells

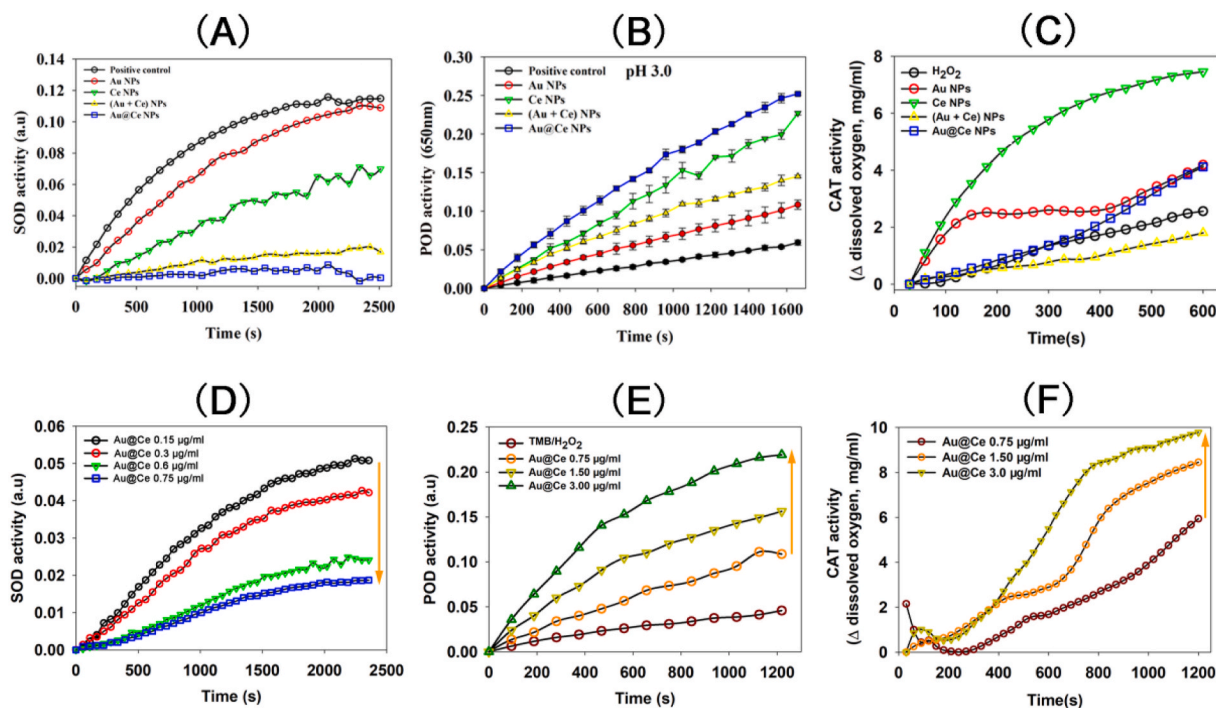AML is a clonal malignant proliferative disease of myeloid blasts of

Fig. 2. SOD-like, POD-like and CAT-like activity of Au@Ce NPs. (A) Curves of SOD activity to show the normalized absorbance variation with time at 560 nm wavelength in NPs/NBT/(Xan + XOD)-generated $O_2\bullet$- systems, in the buffer with pH 7.4. The steps were carried out according to the Kit instructions, and the concentration of nano-agents is as (Au, 1.5 μg/ml, Ce 1.5 μg/ml, Au + Ce, 1.5 μg/ml). (B) Curves of POD activity to show absorbance variation with time at 650 nm wavelength in NPs/TMB/H_2O_2 systems, in the buffer of pH 3.0. The samples contained 0.15 M H_2O_2, 0.2 mg TMB, and 0.4 ml buffer (pH 3.0), as well as the concentration of nano-agents is as (Au, 1.5 μg/ml, Ce 1.5 μg/ml, Au + Ce, 1.5 μg/ml). (C) Curves of CAT activity to show the variation dissolved oxygen concentration with time in NPs/H_2O_2 by a dissolved-oxygen electrode, in the buffer with pH 7.4. The detection system was in 5 ml buffer solution, H_2O_2 concentrations is 0.1 M/L, nano-agents nano-agents is as (Au, 0.75 μg/ml, Ce 0.75 μg/ml, Au + Ce, 0.75 μg/ml). (D) Concentration-dependent SOD curves of Au@Ce NPs. (E) Concentration-dependent POD curves of Au@Ce NPs. (F) Concentration-dependent CAT curves of Au@Ce NPs.

the hematopoietic system. Cell proliferation is strictly controlled by cell cycle progression [39,40]. A complete cell cycle is composed of early DNA synthesis (G1 phase), DNA synthesis (S phase), late DNA synthesis (G2 phase), and mitosis (M phase). The cell cycle starts from G1 phase and ends at M phase. ROS is indispensable for the proliferation and differentiation of normal cells and is a potential driving force to promote the cell cycle forward [21]. Interestingly, cellular ROS fluctuate regularly with changes in the cell cycle. ROS levels are lower in the G1 phase, as the cell cycle progresses, the ROS levels continue to rise, reaching a peak in the M phase [41]. After cell division, the ROS level drops sharply to the low level again at the G1 phase. Tumor cells produce excessive ROS and maintain a high oxidative stress state, which can eventually lead to active tumor cell metabolism and cell cycle checkpoint function inhibition, endowing tumor cells to have the stronger proliferation ability than normal cells of the same kind [41,42]. Accordingly, over-expressing CAT or glutathione peroxidase (GPX) to eliminate endogenous H_2O_2 can block cell cycle at G0/G1 phase and reduce cell DNA synthesis [43,44]. As a result, scavenging excessive ROS in tumor cells can exert the effect in inhibiting cell proliferation [12,14].

Thus, excellent ROS scavenging ability of Au@Ce NPs has the potential to arrest the cell cycle and proliferation of AML cells. We first evaluated the effect of treatment time on cell viability. These nanoparticles did not show acute cytotoxicity, reflecting in no obvious inhibition of cell viability after treatment for 3 h and 6 h (Fig. 6A). However, after 12 h and 24 h, Ce NPs, (Au + Ce) NPs and Au@Ce NPs all induced the significant decrease of cell viability, which is consistent with the removal of ROS (Fig. 6A and B, C). Consequently, the cell cycle changes were detected after 6 h and 24 h treatment. Interesting, Au NPs, Ce NPs, (Au + Ce) NPs and Au@Ce NPs played different roles in intervening cell cycle. In addition to Ce NPs, other groups significantly promoted the S phase but suppressed the G2 phase after 6 h treatment. During this time,

Ce NPs showed no effect on cell cycle. After 24 h of treatment, whereas Au@Ce NPs almost completely arrested cell cycle in G1 phase and restricted the progress of S phase and G2 phase. However, the other three groups promoted the S phase without effect on G1 phase, but all of them significantly inhibited cell cycle progression in G2 phase, suggesting the more excellent ability of Au@Ce NPs in arresting cell cycle (Fig. 6B and C).

Subsequently, we examined the corresponding cell proliferation and apoptosis respectively by Edu Kits and Apoptosis Kits. As shown in Fig. 6D, the proliferation of Edu-labeled cells was observed by fluorescence microscope. Au@Ce NPs obviously inhibited the S-phase progression compared to the controls and other three kinds of treatment (Fig. 6D). At the same time, compared to Ce NPs groups and the mixed (Au + Ce) NPs groups, Au@Ce NPs induced the largest proportion of apoptosis by flow cytometry and PI-staining fluorescence microscopy (Fig. 6E–G). In order to further prove that the inhibition of cell proliferation and induction of apoptosis by Au@Ce NPs is due to its effective scavenging of intracellular ROS, we examined the correlation between antioxidant enzymes (Catalase, SOD1 and SOD2), mitochondrial complex (Ndufs1, SDHB and Uqcrfs1), key proteins in controlling cell cycle (Akt and Cyclin D1) and the MAPK pathway proteins (JNK, p38 and Erk). During the 48 h of treatment by Au@Ce NPs, (SOD1 and SOD2), (Akt and Cyclin D1) and JNK MAPK expression level decreased in time-dependent manner (Fig. 6H and Fig. S13). The continuous decrease of SOD1 and SOD2 proteins indicated that the intracellular $O_2\bullet$- in HL-60 cells was eliminated all the time, while the sustained down-regulation of (Akt and Cyclin D1) and JNK MAPK revealed the blockage of cell cycle signal and cell proliferation signal. Thus, after 24 h of treatment by these nano-agents, we demonstrated again that above proteins were all down-regulated except Erk for Au@Ce NPs treatment (Fig. 6I and Fig. S14). Consistent with this, the phosphorylation of Akt and MAPK were also
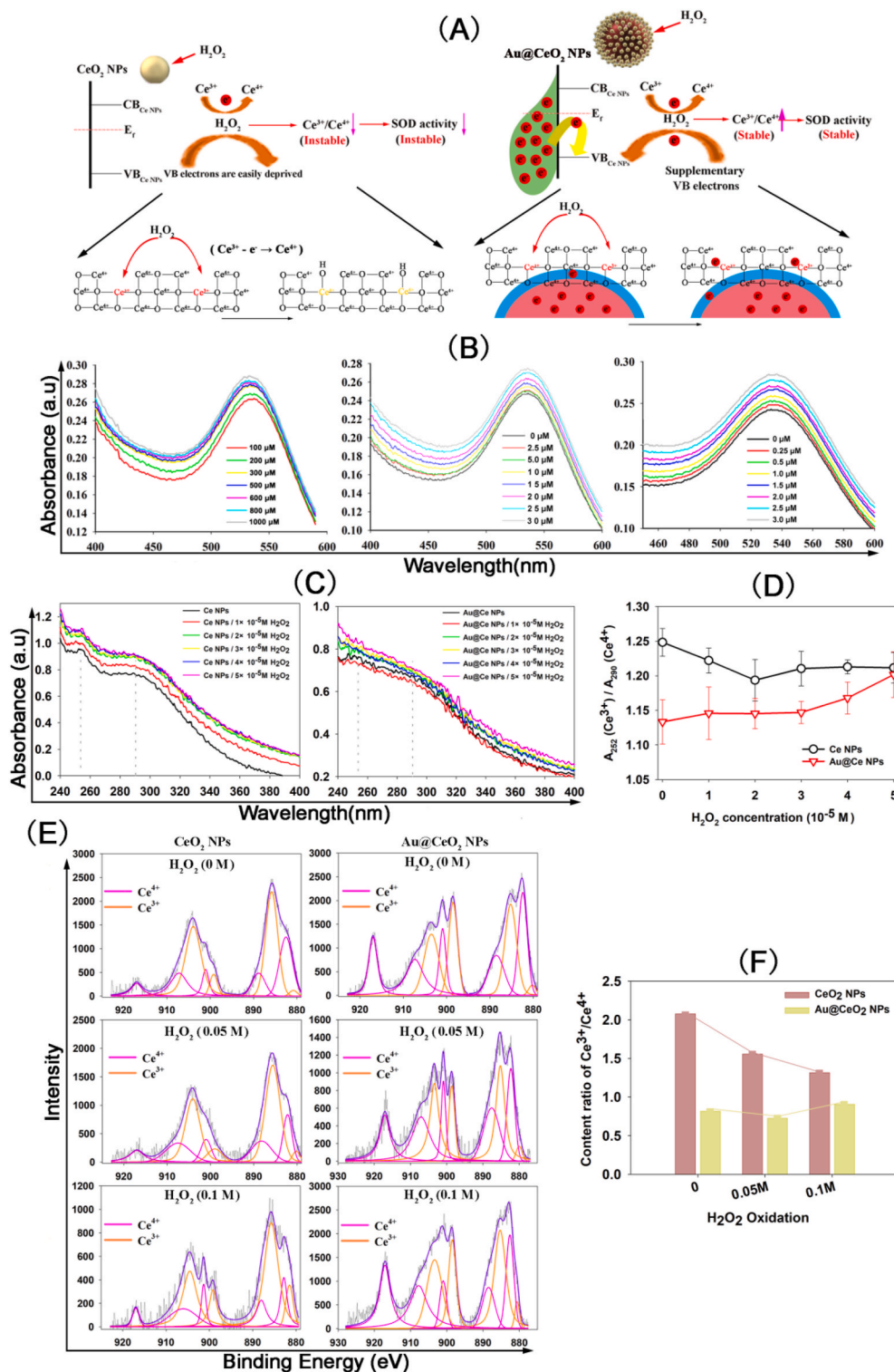
Fig. 3. Au@Ce NPs can maintain the stability of Ce^{3+}/Ce^{4+}. (A) Schematic diagram to show the mechanism that after assembly of Au NPs and Ce NPs, Au NPs can transmit electron to Ce NPs to maintain the ratio of Ce^{3+}/Ce^{4+} upon the oxidation by H_2O_2, Au@Ce NPs consequently have high-performance SOD activity even though in a high oxidation stress. (B) UV–Vis spectra of Au@Ce NPs treated with different concentrations of H_2O_2. (C) UV–Vis spectra of Ce NPs and Au@Ce NPs treated with different concentrations of H_2O_2, and (D) the ratio of corresponding absorbance at 252 nm and at 290 nm, approximate to the ratio of Ce^{3+}/Ce^{4+}. (E) and (F) Freeze-dried powder of Ce NPs and Au@Ce NPs were respectively treated by H_2O_2 of corresponding concentration, the mixed solution was then dried by blower to get the dried products, which were then tested by XPS to count the changes of Ce^{3+}/Ce^{4+} ratio.

diminished after treatment (Fig. S15) Ce NPs induction also decreased the expression of antioxidant enzymes but it was less significant than Au@Ce NPs. More critically, Au@Ce NPs almost completely blocked the expression of Akt and MAPK proteins, which was not observed in CeO_2-treated HL60 cells. While malignant proliferation of AML cells are regulated by ROS/Akt/CyclinD1-mediated cell cycle signal and ROS/MAPK-mediated cell proliferative signal. Therefore, the blocking of ROS signal by Au@Ce NPs can arrest cell cycle and inhibit proliferation of AML cells.

2.7. Au@Ce NPs as an anti-leukaemic therapy

Thus, we evaluated the treatment for HL60-beared BALB/c nude mice. Fig. 7A presents the procedures about the establishment of mice subcutaneous tumor and therapy. On the third day after transplantation and tumorigenesis, nano-reagents were injected intravenously every two days. During the time, the changes of body weight were recorded, and there was no obvious difference between them (Fig. 7B). It is worth noting that these mice have been gaining weight from Day 6, and the
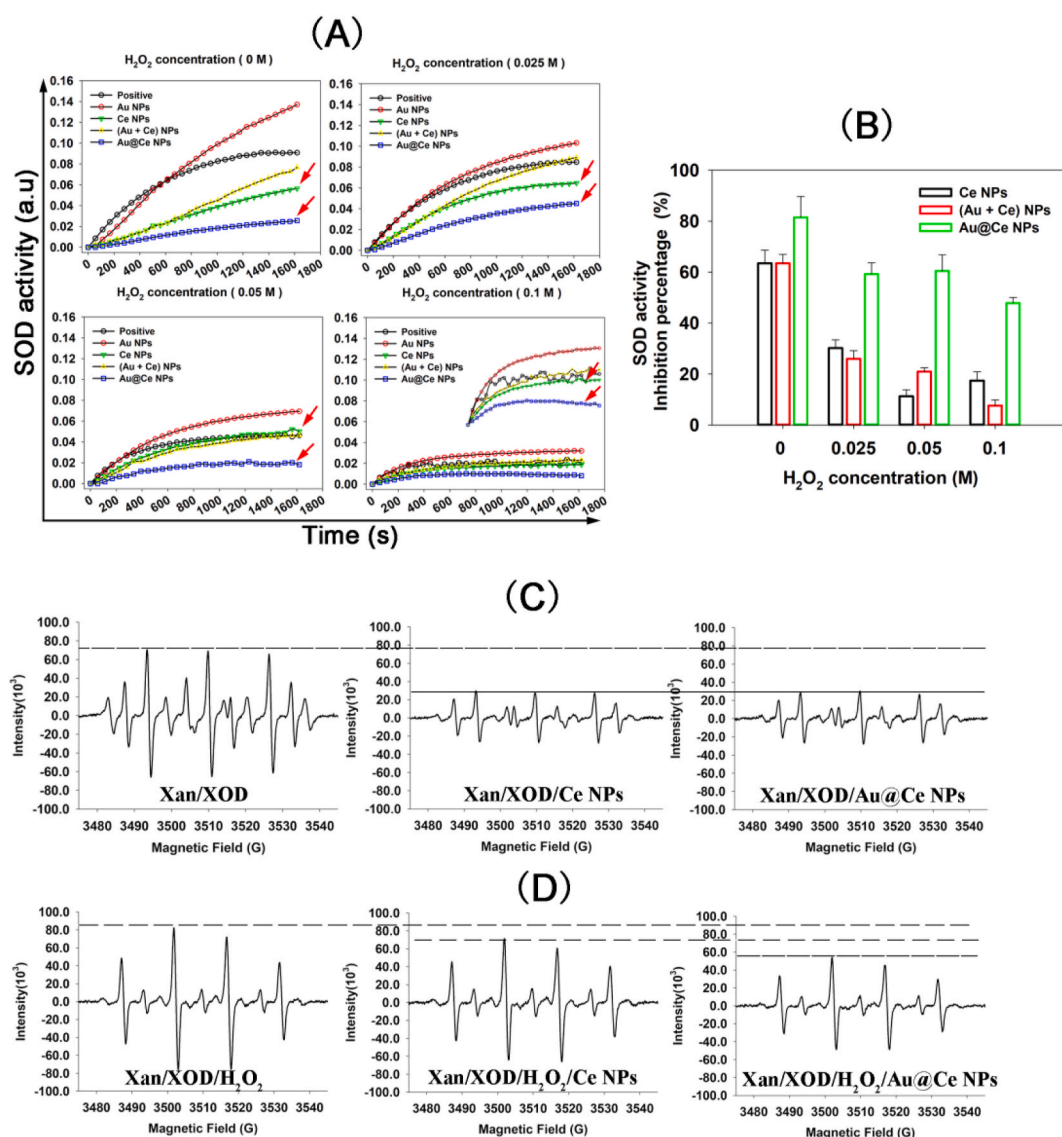
Fig. 4. High-performance SOD activity of Au@Ce NPs. (A) and (B) Effect of H_2O_2 oxidation on the SOD activity of Ce NPs, (Au + Ce) NPs and Au@Ce NPs was tested by the superoxide dismutase activity assay kit. (C) DMPO/EPR was used to evaluate the SOD activity of Ce NPs and Au@Ce NPs, Xanthine (Xan) and xanthine oxidase (XOD) was mixed to generate the $O_2\bullet-$. (D) DMPO/EPR was used to evaluate the effect of H_2O_2 oxidation on the SOD activity of Ce NPs and Au@Ce NPs, Xan/XOD was used to generate the $O_2\bullet-$.

increase was more significant in the saline-treated group. According to the tumor size recorded, Ce NPs, (Au + Ce) NPs, Au@Ce NPs all suppressed the growth of tumors, especially Au@Ce NPs administration achieved the most significant effect in restraining tumor growth (Fig. 7C and D). Mice in saline group died in succession from the second week. After three weeks of treatment, all mice were sacrificed to extract the tumors and main visceral organs, of course, the dead mice during the time were deal with in the same way. The results of tumor volume measurement demonstrated again that Au@Ce NPs administration had significant tumor inhibitory effect, as well as Ce NPs and (Au + Ce) NPs also showed inhibitory effect on tumor growth, which was consistent with their ability to arrest cell cycle and induce apoptosis (Fig. 7E and F). Critically, saline-treated control mice had severe splenomegaly. However, after administration, the spleens of mice were significantly smaller than that of saline group, and the change of spleens in these mice treated by Au@Ce NPs was the smallest (Fig. 7G and H). And the liver tissues also exhibited the similar phenomenon (Data not shown). As a result, the survival time of mice was significantly prolonged after treatment with nano-agents, where Au@Ce NPs treatment group got the longest lifetime

(Fig. 7I).

2.8. Evaluation in vivo

Extracted tissues were then sectioned and stained with H&E. No significant changes were observed in the heart, lung, and kidney tissues among these five groups of mice (Fig. S16). However, there was difference between their livers and spleens. In these livers, obvious leukocyte infiltration can be observed by H&E staining, where the saline group, Au NPs group and Ce NPs group are more serious than that in (Au + Ce) NPs group and Au@Ce NPs group (Fig. 8A). In the corresponding spleens, except the spleens treated by Au@Ce NPs, other four groups of spleens were with diffused white pulp and weird shape (Fig. 8A). In other words, Au@Ce NPs treatment group alleviated against the leukocyte infiltration in the liver and spleen tissue, consistent with the previously observed phenomenon of protected liver and spleen. To further prove the inhibitory effect of Au@Ce NPs on tumor growth, Ki67 and Cyclin-D1 positive cells were respectively stained in tumor tissues by immunohistochemistry, two kinds of markers to index cell proliferation where Ki67 reflects
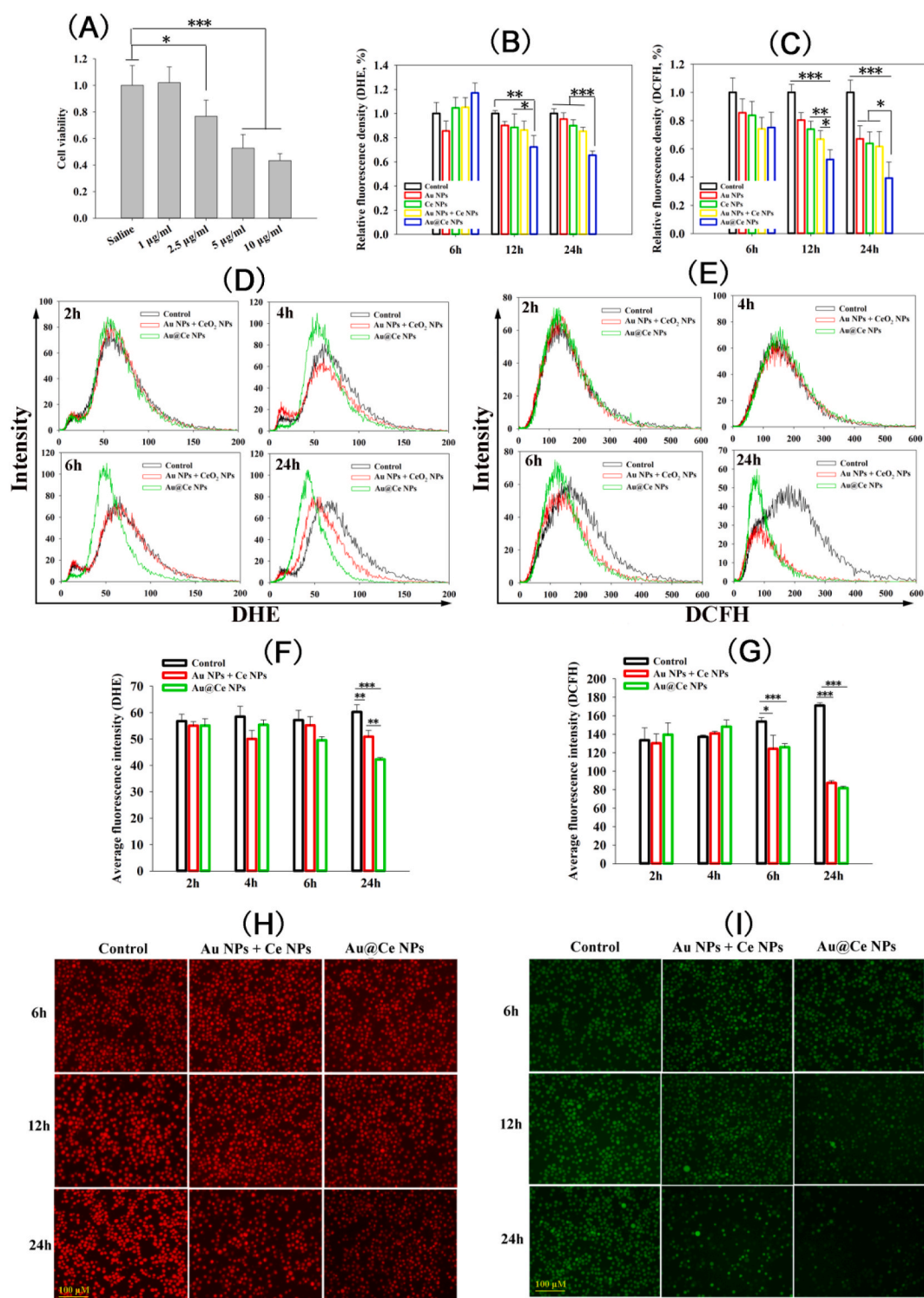
Fig. 5. Scavenging intracellular ROS in HL-60 cells. (A) HL-60 cells were treated by Au@Ce NPs of different concentration for 24 h, saline treatment was as the control. Cell viability was examined by cck8. (B) and (C) HL-60 cells were incubated with Au NPs, Ce NPs, (Au + Ce) NPs and Au@Ce NPs respectively for 6 h, 12 h, 24 h. DHE probes and DCF-DA probes were respectively used to label the level of $O_2\bullet-$ and ROS by the microplate reader. (D) and (E) HL-60 cells were incubated with (Au + Ce) NPs and Au@Ce NPs respectively for 2 h, 4 h, 6 h, 24 h. DHE probes and DCF-DA probes were respectively used to label the level of $O_2\bullet-$ and ROS by the flow cytometry. Their average fluorescence intensity was shown in (F) and (G). And after treatment for 6 h, 12 h and 24 h, DHE-labeled and DCFH-labeled cell fluorescence microscopy was respectively shown in (H) and (I). Data was shown as mean ± SD. *p < 0.05; **p < 0.01; ***p < 0.001.

cell proliferation and Cyclin-D1 indicates cell cycle. H&E staining showed the tumor shapes (Fig. 8B), but we didn't find a significant difference. Interestingly, Ki67 positive cells were less in Au@Ce NPs treated tumor than the other four groups of tumors (Fig. 8C). As well, Cyclin-D1 positive cells were also similarly less in these tumors treated

by Au@Ce NPs (Fig. 8D). Furthermore, we extracted the tumor proteins and the expression of related proteins was detected by immunoblotting. Consistent with that in vitro, the corresponding tumor in Au@Ce NPs treatment groups showed the down-regulation of cell cycle proteins (Akt and Cyclin D1) and the blockage of p38 MAPK pathway (Fig. S17). These
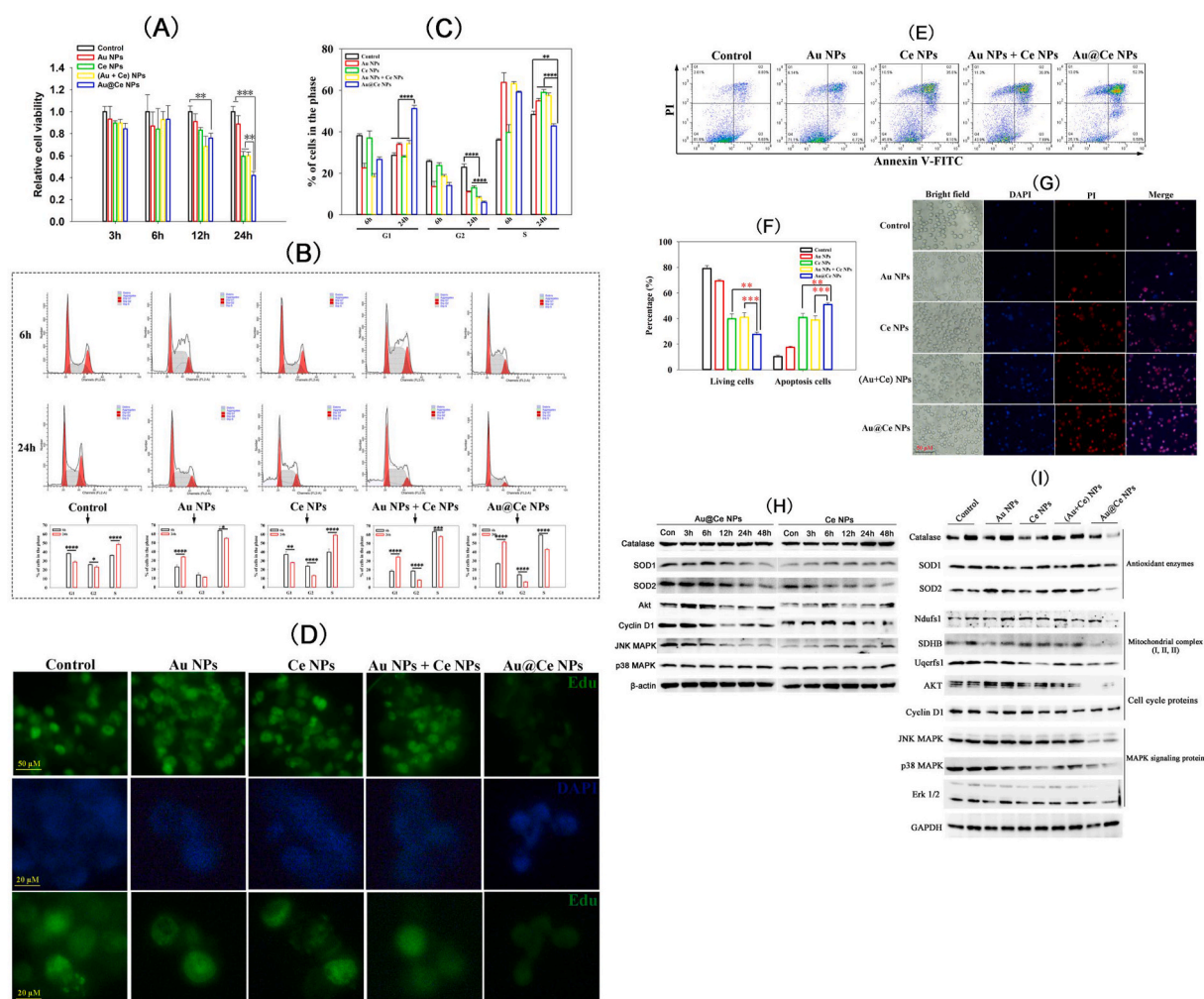
Fig. 6. Au@Ce NPs arrested cell cycle and inhibited proliferation of HL-60 cells. (a) HL-60 cells were respectively treated by Au NPs, Ce NPs, (Au + Ce) NPs and Au@Ce NPs for 3 h, 6 h, 12 h, 24 h. Relative cell viability compared to the control was examined by cck8. (B) Flow cytometry analysis based on PI staining to evaluate the changes of cell cycle after HL-60 cells were treated by nano-agents for 6 h and 24 h, and (C) shows the statistical results corresponding to G1 phase, S phase and G2 phase. HL-60 cells were treated by nano-agents for 24 h, (D) Edu-labeled cell proliferation was observed by fluorescence microscopy, (E) and (F) cell apoptosis was detected by flow cytometry and apoptosis assay kit, (G) PI staining to determine cell damage and death. (H) Time-dependent proteins expression level was confirm to evaluate the effect on antioxidant enzymes (CAT, SOD1, SOD2), cell cycle signaling (Akt/Cyclin D1) and MAPK signaling (JNK MAPK, p38MAPK) via immunoblotting, after HL-60 cells were respectively treated by Ce NPs and Au@Ce NPs. (I) After 24 h treatment by nano-agents, proteins expression level was confirm to evaluate the effect on antioxidant enzymes (CAT, SOD1, SOD2), Mitochondrial complex (Ndufs1, SDHB, Uqcrfs1), cell cycle signaling (Akt/Cyclin D1) and MAPK signaling (JNK MAPK, p38MAPK, Erk1/2) via immunoblotting. Data was shown as mean ± SD. *$p < 0.05$; **$p < 0.01$; ***$p < 0.001$; ****$p = 0.000$.

data suggested that these tumors were poor proliferation ability after treatment by Au@Ce NPs.

2.9. Au@Ce NPs prolonged the survival period in systemic AML model mice

Thus, we had implemented systemic AML model in NOD SCID mice and the treatment of Au@Ce NPs has indeed delayed the proliferation of AML cells in mice and prolonged the survival period. As shown in Fig. S18, NOD SCID mice were injected with HL-60 cells (5×10^5) through the tail vein. The administration of Au@Ce NPs was started on the tenth day, one time every 2–3 days for one month. The normal saline was administered as the control (n = 6). On the 15th and 30th days, peripheral blood and bone marrow blood were respectively stained by WRIGHT-GIEMSA (Fig. S18a), promyelocytes cells can be observed in bone marrow and peripheral blood. On the 30th day, the promyelocytes cells in the bone marrow increased significantly, and some cells were dividing and proliferating. On the 30th days, FITC-CD33-labeled flow cytometry results of peripheral blood were conducted to determine the

proliferation of AML cells. It indicates that Au@Ce NPs administration inhibited the proliferation of HL-60 in mice (Fig. S18b). Bone marrow blood was stained by WRIGHT-GIEMSA when the mice in the saline group were in a state of dying, and at the same time, the bone marrow blood in Au@Ce-treated mice was also stained. As a result, proliferating promyelocytes were full in the bone marrow of lower limbs of the dying mice in saline group, but much less promyelocytes were observed in Au@Ce-treated mice (Fig. 9a). Meanwhile, survival time of mice was shown in Fig. 9b and the corresponding mice pictures of different time were taken (Fig. S18 c), Au@Ce NPs treatment significantly delayed the survival of mice. The red arrow marks the paralysis of the mouse's lower limbs.

AML is a blood-cloned malignant proliferative disease of hematopoietic system, where elevated levels of steady-state ROS modulate the expression of critical kinases, phosphatases and redox-sensitive transcription factors, involving in the malignant proliferative [15]. Therapeutic strategies targeting intratumoral ROS have been widely applied in radiotherapy and chemotherapy clinically. In terms of chemotherapy drugs, Elesclomol [45] and Cisplatin [46] were successful therapeutic
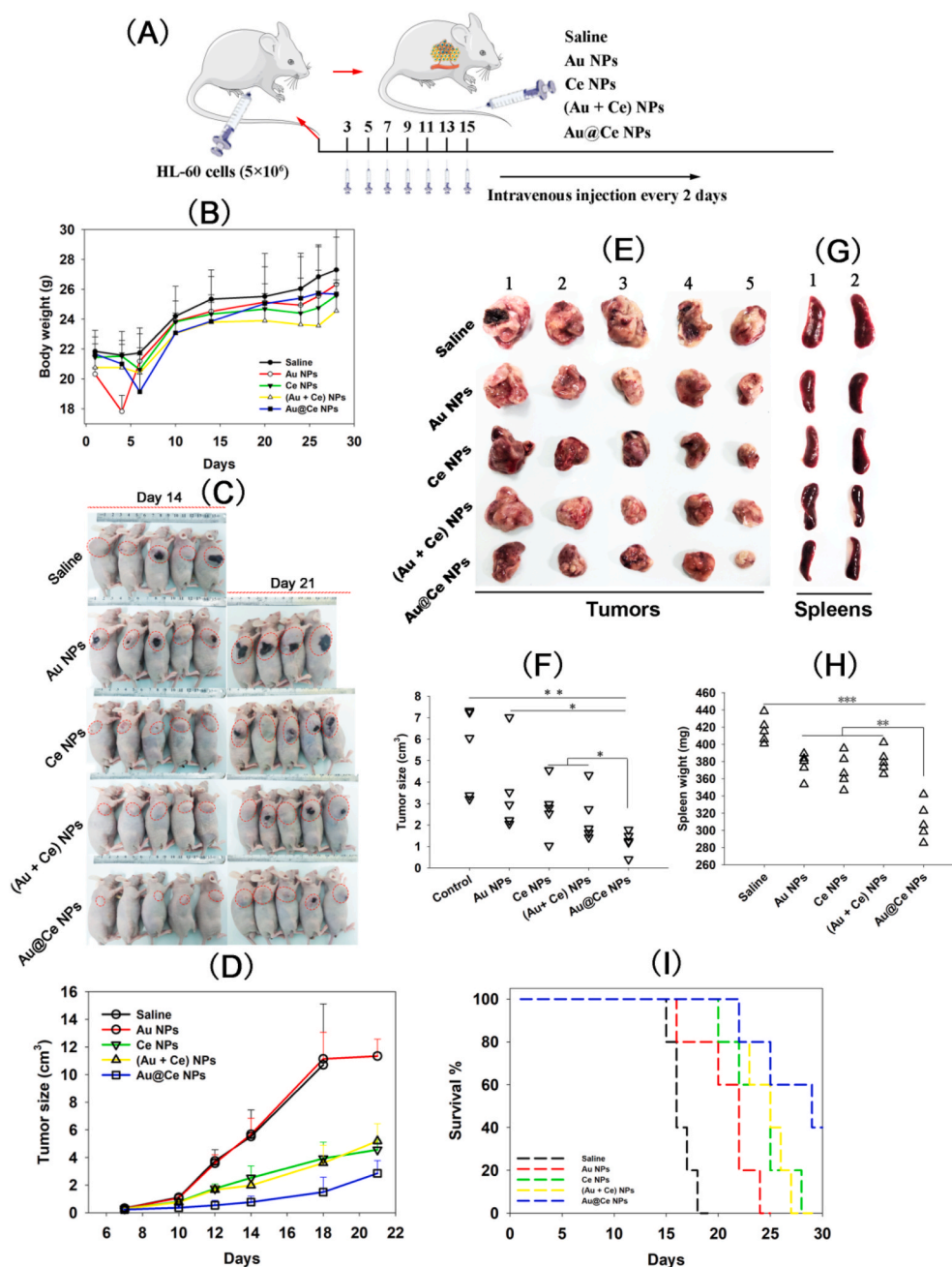
Fig. 7. Au@Ce NPs as an anti-leukaemic therapy. (A) Flow chart of treatment for HL60-beared BALB/c nude mice (5 groups, n = 5). (B) Changes in body weight of mice within 30 days. (C) Photos of tumor-beared mice after treatment for two weeks and three weeks. (D) The tumor size changes after treatment. (E) and (F) After treatment of three weeks, all mice were sacrificed to get the tumors and measure their size. (G) and (H) Mouse spleens were stripped to take photos and weighed them. (I) For the second batch of mice, changes in the survival rate of mice over time (5 groups, n = 5). Data was shown as mean ± SD. *p < 0.05; **p < 0.01; ***p < 0.001.

drugs based on ROS, the former has been used for the treatment of melanoma, and the latter was used for multiple tumors. However, these therapies tend to elevate ROS to kill cancer cells. Although the curative effect is significant, it is also accompanied by the problems of easy relapse and drug resistance. This is because the elevated ROS is more susceptible to feedback from the antioxidant system [23,47]. The development of artificial enzymes, especially the discovery of nanozyme, provides a choice for tumor therapy by ROS intervention, based on their high efficiency, stability and controllability. Kong et al. recently reported the synergistic treatment of leukemia by the mimetic POD enzyme of Fe_3O_4@Pt NPs and CXCR4 antagonist [6]. In the mildly acidic lysosome micro-environment, highly toxic ROS was generated through the sequential catalytic reactions of Fe_3O_4@Pt to trigger AML cells apoptosis after targeting to the CXCR4 receptor through the CXCR4 antagonist, leaving the normal cells unharmed. Additionally, FDA-approved ferumoxytol was reported to display the anti-leukemia

efficacy through ROS, where the main ingredient of ferumoxytol is iron oxide nanoparticles [48]. These studies imply that the intervention of ROS in leukemia cells by artificial nanozymes is beneficial to the treatment of leukemia.

Unlike iron-based nanozymes that trigger the POD-like reaction, in physiological pH conditions, we found Au@Ce nano-system mainly exerted its SOD enzyme activity. Although, Sanjay Singh et al. reported assembled Au/CeO_2 exhibited the weaker POD-like activities in physiological pH, their Au/CeO_2 caused a decrease in hydroxyl radical (HO•) formation instead, proving the ability of free radical scavenging [33]. In addition to the effect of pH, the enzyme activity of Ce NPs and Au@Ce NPs was also dependent on the ratio of Ce^{3+}/Ce^{4+}, the higher the proportion of Ce^{4+}, the stronger the POD enzyme activity is, and the higher the proportion of Ce^{3+}, the stronger the SOD activity is. Based on our findings, we believe that the stability of Ce^{3+}/Ce^{4+} ratio is more critical to the enzymatic activity of ceria-based naonzyme, at least for its
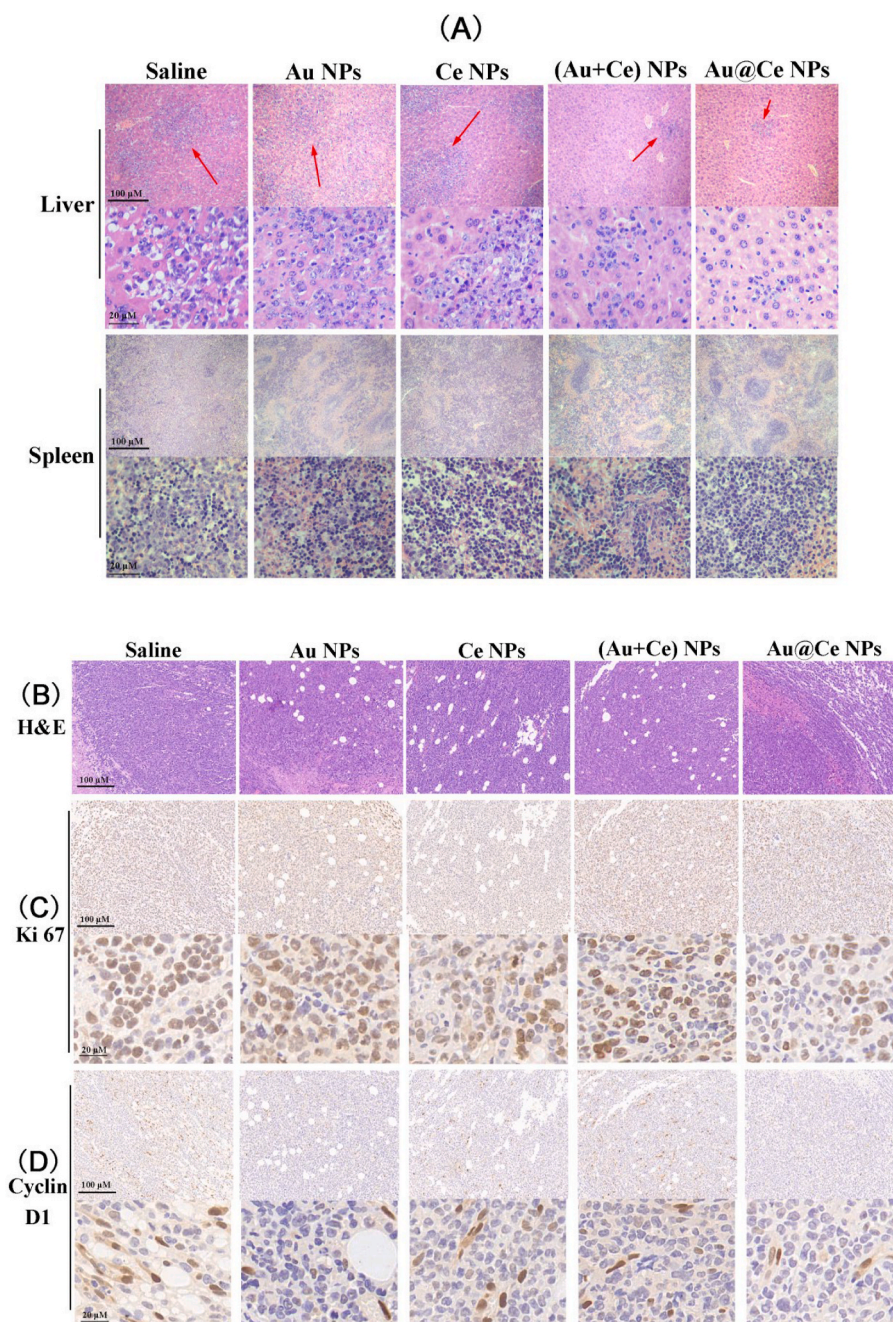
Fig. 8. Evaluation in vivo. (A) Hematoxylin-Eosin staining (H&E) for livers and spleens in these treated mice. (B) H&E staining for tumors in these treated mice. (C) Ki67-labeled immunohistochemistry staining for tumors in these treated mice. (D) Cyclin D1-labeled immunohistochemistry staining for tumors in these treated mice.

SOD-like activity. Theoretically, SOD enzyme should participate in the disproportionation reaction, corresponding to ceria-based NPs, it should be associated with the balance between $Ce^{3+} \rightarrow Ce^{4+}$ (oxidation) and $Ce^{4+} \rightarrow Ce^{3+}$ (reduction), only this disproportionation reaction proceeding stably can exert more efficient SOD activity of ceria NPs. We even suspected the mechanism that the more Ce^{3+} in Ce NPs, the stronger the SOD activity is. Otherwise it is hard to explain why the pure Ce^{3+} ion does not exhibit SOD enzyme activity. Whereas the assembled Au@Ce NPs can transfer the free electrons from the surface of Au NPs to Ce NPs upon the oxidation through the enhanced LSPR, maintaining the stability of Ce^{3+}/Ce^{4+} ratio as well as the SOD-like function. This mechanism can promise the stable SOD enzyme activity of Au@Ce NPs to the greatest extent even in a complex pathological environment, which is of great significance for removing $O_2\bullet-$ and H_2O_2 in AML cells.

In AML cells, ETC and NOXs derived the superoxide anion $O_2\bullet-$ constantly, which is the main oxygen source for other ROS (H_2O_2 and $\bullet OH$) and has a relatively stable source [11,21]. $O_2\bullet-$ can be quickly converted into stable H_2O_2 with the catalysis of SOD1/2 [49]. Higher capability of $O_2\bullet-$ generation by AML cells will consume SOD (SOD1 and SOD2), resulting in the low level of SOD. Elevated homeostasis ROS of $O_2\bullet-$ and the derived H_2O_2 was able to activate MAPKs signaling and Akt/GSK-3/Cyclin cascade, which together played the key role in malignant proliferation and aggressiveness of AML [15]. In this sense, supplement of SOD enzyme to eliminate $O_2\bullet-$ free radicals is beneficial to suppress the proliferative signal in AML cells. In fact, targeting $O_2\bullet-$ or SOD has been reported as a promising approach for AML [7]. However, many fatal shortcomings of natural SOD enzymes limit their clinical use, for example, immunogenicity and extremely short half-life [25].
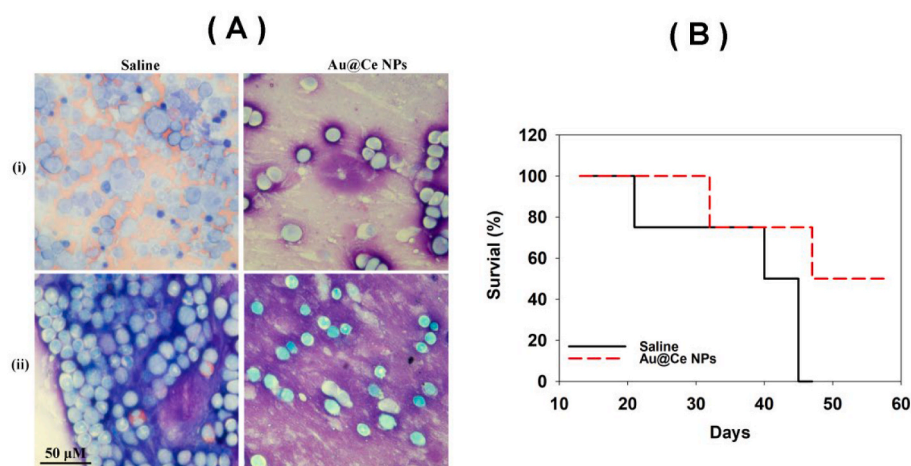
Fig. 9. Au@Ce NPs prolonged the survival period in systemic AML model mice. (A) Bone marrow blood was stained by WRIGHT-GIEMSA when the mice in the saline group were in a state of dying, and at the same time, the bone marrow blood in Au@Ce-treated mice was also stained. (B) Survival time of mice (n = 4).

Therefore, the high-performance SOD-like activity of Au@Ce NPs provided an ideal platform to interfere with the level of intracellular $O_2\bullet-$, which can intermeddle the ROS conversion axis ($O_2\bullet-\rightarrow H_2O_2\rightarrow O_2/HO\bullet$) and ROS level ($O_2\bullet-$ and H_2O_2).

In terms of the utilization of ROS, radiotherapy is more dependent on the toxicity of ROS that was produced by ionizing radiation [50]. Although the therapeutic effect of radiotherapy is remarkable, as the serious side effect, a large amount of generated ROS will cause serious damage to normal tissues. Additionally, ROS excited by radiotherapy requires the oxygen source from tumor tissue, where is actually hypoxic instead [51–53]. Thus, Au@Ce NPs shows the application prospect in radiotherapy. On the one hand, its efficient ability in scavenging ROS can minimize the damage to normal tissue. On the other hand, CeO_2 NPs is characterized with oxygen storage/release that can provide additional oxygen source for hypoxic tumor tissue to generated ROS upon the excitation by radiation [54].

Anyway, the assembly of Au NPs and CeO_2 NPs is valuable, especially the free electron compensation capability of Au NPs surface is helpful to maintain the stability of Ce^{3+}/Ce^{4+} ratio on the surface of CeO_2 NPs, preserving the stability of mimetic enzyme activity. Importantly, this continuous free radical scavenging ability is just what conventional antioxidants such as vitamin C/E lack. In conclusion, assembled Au@Ce NPs show the high-performance SOD activity and ROS relay effect, promising a great potential in the treatment of AML and oxidative stress disorders.

3. Conclusions

SOD-like activity of Ce NPs is drived by Ce^{3+}/Ce^{4+}, endogenous oxidative stress can oxidize Ce^{3+} to reduce the ratio of Ce^{3+}/Ce^{4+}, inactivating the SOD activity of Ce NPs. Au@Ce NPs, assembled by Au NPs and Ce NPs, exhibited high-performance of SOD mimetic enzyme activity. Upon the oxidation of H_2O_2, Ce NPs supported by nano-Au can acquire the electrons from Au NPs through the enhanced LSPR, maintaining the stability of Ce^{3+}/Ce^{4+}. Thus, Au@Ce NPs exhibited high-performance SOD activity even in the high oxidation conditions. High-performance SOD activity of Au@Ce NPs effectively scavenged $O_2\bullet-$ and the derived ROS in AML cells, which are the important signaling source to drive AML cell proliferation and accelerate their cell cycle progression. Thus, Au@Ce NPs treatment significantly inhibited the cell proliferation and induced apoptosis by arresting cell cycle at G1 phase greatly. Importantly, this treatment strategy also showed therapeutic effect for subcutaneous transplantation of AML model. In particular, it shows a satisfactory result in preventing the leukocyte infiltration of liver and spleen. Au@Ce NPs with high-performance SOD activity

provides a choice for the treatment of AML, and importantly, it shows the potential for ROS removal in other diseases safely and efficiently.

4. Experimental section

4.1. Au NPs synthesis

A proper amount of dextran (67.5 mg, Mw:40000) was dissolved into ultra-pure water (5 mL), stirring it after adding 215 μL chlorogold acid (1 %). The mixed solution was heated in 80 °C water bath for 5min. At this time, 2 mg disodium citrate was then dissolved into above solution and heated for another 20 min until the solution is claret. The Au NPs was washed by ultrafiltration and filtered by 220 nm ultrafiltration membranes.

4.2. Ce NPs synthesis

CeO_2 colloidal solution was successfully synthesized via a hydrothermal co-precipitation procedure. Cerium nitrate hexahydrate and dextran (1:3, mass ratio) were mixed in pure water and stirred well. Then adding an appropriate amount of ammonia and heating the mixed solution in a 65 °C water bath. The colloidal solution were dialyzed by dialysis bag and then filtered by 220 nm ultrafiltration membranes.

4.3. Au@Ce NPs synthesis

Au@Ce NPs was prepared by one-pot method. Sodium chloride solution, cerium nitrate hexahydrate, dextran and chlorogold acid were mixed and keep warm in 60 °C oil bath for 5 min. Add appropriate amount of ammonia and then stir it in 60 °C oil bath for 1 h. The nanoparticles was then precipitated by acetone and re-dissolved by ultrasound after washed. The Au@Ce NPs was washed by ultrafiltration and filtered by 220 nm ultrafiltration membranes.

4.4. Characterization

Transmission electron microscopy (TEM) analysis was carried out using a JEOL 2100 microscope. Energy dispersive spectrometer (EDS) analysis was carried out using a Zeiss Ultra Plus field emission scanning electron microscope (SEM). Quantification of Au and Ce were performed using inductively coupled plasma-optical emission spectroscopy (ICP-OES, PerkinElmer Optima 4300 DV, Shelton, CT). UV–vis–NIR absorption spectra were recorded using a spectrophotometer (UV-3600) (Shimadzu, Kyoto, Japan). The hydrodynamic diameter was measured by a Zetasizer Nano-ZS (Malvern Instruments). The powder XRD patterns

were acquired on an AXS D8 advance (Bruker, Germany). Microplate Reader was from Infinite M200 (TECAN, Switzerland).

4.5. ROS analysis by flow cytometry

AML cells were cultured and treated according to different conditions. These cells were collected and re-suspended in fresh 1640 serum free and phenol red free medium, which were then co-cultured by DHE probe (S0063, Beyotime Biotechnology), DCFH probe (S0033S, Beyotime Biotechnology) and HPF probe with appropriate concentration. After the cells were incubated in the incubator for appropriate time, the labeled-cells were detected by flow cytometer.

4.6. PI-labeled cell cycle by flow cytometry

Collect the required cells and wash them. Re-suspend the collected cells in 500 μL pre-cooled PBS buffer, centrifuge the solution at 1000 rpm for 5 min and remove the supernatant. Re-suspend the cells with 500 μL of pre-chilled ethanol and fix them at 4 °C for 30 min. After fixing, centrifuge these cells at 1000 rpm for 5 min and remove the supernatant again. Re-suspend the collected cells with 500 μL pre-cooled PBS buffer and then centrifuge them again. After removal of the supernatant, re-suspend these cells with 500 μL RNase A (100 μg/mL), and then incubate them for 30 min at 37 °C to fully degrade the RNA in the cells. Finally, collect the cells by centrifugation, re-suspend them with 200 μL PI staining solution (50 μg/mL) and then incubate them on ice for 30 min in the dark. All groups of cells were then tested on the machine.

4.7. Apoptosis analysis by flow cytometry

AML cells were cultured and treated at different conditions, which were collected by centrifugation at $100 \times g$ for 5 min and resuspended in a binding buffer (10 mM HEPES, 140 mM NaCl, 2.5 mM CaCl$_2$) at room temperature at a density of 1×10^6 cell/ml. The cells (100 μL) were stained with 5 μL of Annexin-V-FITC and 5 μL of PI in a culture tube and incubated at room temperature in the dark for 15 min by FITC Annexin V Apoptosis Detection Kit 1(BD Pharmingen™). After addition of 400 μL binding buffer, the cells (~10,000 cells per assay) were then analyzed by flow cytometer within 1 h period.

4.8. Animal protocol

BALB/c nude male mice were provided by the Animal Center of Qinglongshan (Nanjing, China). All animal experiments were carried out conforming to the Guideline for Animal Experimentation in agreement with the animal care committee of Southeast University. For acute myeloid leukemia (AML) mice construction, the BALB/c nude male mice were subcutaneously transplanted with 1 mL HL-60 cell suspension in PBS (5×10^6 cells). After transplantation for 7 days, Au NPs, Ce NPs, (Au + Ce) NPs and Au@Ce NPs were administered respectively one time every two days via the tail vein. Saline injected with equal volume was as the control group. Among the processes, body weight and tumor size of these mice were monitored and the survival rate changes was also counted. Finally, they were harvested for pathological or pharmacological analysis.

NOD-SCID male mice were provided by GemPharmatech Co., Ltd. (Nanjing, China). All animal experiments were carried out conforming to the Guideline for Animal Experimentation in agreement with the animal care committee of Southeast University. For acute myeloid leukemia (AML) mice construction, the mice were transplanted with 0.2 mL HL-60 cell suspension in PBS (5×10^5 cells) via the tail vein. After transplantation for 10 days, Au@Ce NPs were administered respectively one time every 2–3 days via the tail vein. Saline injected with equal volume was as the control group.

4.9. H&E staining

Briefly, the mice were sacrificed and the tissues like heart, liver, spleen, lung, kidney, and bone marrow were excised and fixed in 4 % polymethyl alcohol solution. Thereafter, the tissues were treated by a series of processes such as dehydration, immersion in paraffin, and embedding and sectioned at a thickness about 3–5 μm. In succession, the slices were stained by hematoxylin-eosin and finally observed via optical microscopy.

4.10. Western blot analysis

Cultured cells were washed twice with PBS and then lysed in RIPA lysate buffer (Beyotime, Poo13C, China). Insoluble materials from cultured cell lysates were removed by a brief centrifugation at 4 °C, and the supernatants were subjected to 10 % SDS-polyacrylamide gel electrophoresis and transferred to a polyvinylidene difluoride filter (PVDF) membrane by a transfer apparatus at 300 mA for 1.5 h. The membrane was then blocked with 5 % nonfat milk, followed incubated with primary antibody overnight at 4 °C, washing and then with secondary antibodies for 2 h at room temperature (RT) and scanned with the imaging system (Tanon, 4600SF).

4.11. Statistical analysis

The statistical analysis was carried out by SPSS software via the Student's t-test. All of the data in this work were expressed as the mean value with standard deviation. Statistical significance was expressed as follows: $*p < 0.05$; $**p < 0.01$; $***p < 0.001$.

Declaration of competing interest

The authors declare no conflict of interest.

CRediT authorship contribution statement

Yuxiang Sun: Writing – original draft, Experimental design and operation, process planning including implementation, writing, contribution, revision, etc. **Xin Liu:** Experimental operation of ROS detection. **Lei Wang:** Guidance on experimental design and animal experiments. **Li Xu:** Responsible for cell culture and detection of biological samples. **Kunliang Liu:** Participating in the synthesis of nanoparticles. **Lei Xu:** Participating in the implementation of animal experiments. **Fangfang Shi:** Providing some references about the basic knowledge of tumors. **Yu Zhang:** Funding acquisition, Providing a part of the funds. **Ning Gu:** Providing the experimental platform. **Fei Xiong:** Funding acquisition, Undertaking the main funds of the project and responsible for the overall control of experiments.

Acknowledgement

Appendix A. Supplementary data

Supplementary data to this article can be found online at https://doi.org/10.1016/j.bioactmat.2021.08.012.

References

[1] J.N. Saultz, R. Garzon, Acute myeloid leukemia: a concise review, J. Clin. Med. 5 (2016).

[2] H. Hackl, K. Astanina, R. Wieser, Molecular and genetic alterations associated with therapy resistance and relapse of acute myeloid leukemia, J. Hematol. Oncol. 10 (2017) 51.

[3] C. Rautenberg, U. Germing, R. Haas, G. Kobbe, T. Schroeder, Relapse of acute myeloid leukemia after allogeneic stem cell transplantation: prevention, detection, and treatment, Int. J. Mol. Sci. 20 (2019).

[4] H. Zhang, H. Fang, K. Wang, Reactive oxygen species in eradicating acute myeloid leukemic stem cells, Stem Cell Invest. 1 (2014) 13.

[5] F. Zhou, Q. Shen, F.X. Claret, Novel roles of reactive oxygen species in the pathogenesis of acute myeloid leukemia, J. Leukoc. Biol. 94 (2013) 423–429.

[6] F. Kong, H.Y. Bai, M. Ma, C. Wang, H.Y. Xu, N. Gu, et al., Fe3O4@Pt nanozymes combining with CXCR4 antagonists to synergistically treat acute myeloid leukemia, Nano Today (2021) 37.

[7] P. Huang, L. Feng, E.A. Oldham, M.J. Keating, W. Plunkett, Superoxide dismutase as a target for the selective killing of cancer cells, Nature 407 (2000) 390–395.

[8] T.K. Er, E.M. Tsai, S.H. Wu, W. Chiang, H.C. Lin, S.F. Lin, et al., Antioxidant status and superoxide anion radical generation in acute myeloid leukemia, Clin. Biochem. 40 (2007) 1015–1019.

[9] P.S. Hole, J. Zabkiewicz, C. Munje, Z. Newton, L. Pearn, P. White, et al., Overproduction of NOX-derived ROS in AML promotes proliferation and is associated with defective oxidative stress signaling, Blood 122 (2013) 3322–3330.

[10] P.S. Hole, L. Pearn, A.J. Tonks, P.E. James, A.K. Burnett, R.L. Darley, et al., Ras-induced reactive oxygen species promote growth factor-independent proliferation in human CD34(+) hematopoietic progenitor cells, Blood 115 (2010) 1238–1246.

[11] J.R. Sillar, Z.P. Germon, G.N. De Iuliis, M.D. Dun, The role of reactive oxygen species in acute myeloid leukaemia, Int. J. Mol. Sci. 20 (2019).

[12] C. Vignon, C. Debeissat, J. Bourgeais, N. Gallay, F. Kouzi, A. Anginot, et al., Involvement of GPx-3 in the reciprocal control of redox metabolism in the leukemic niche, Int. J. Mol. Sci. (2020) 21.

[13] V. Aggarwal, H.S. Tuli, A. Varol, F. Thakral, M.B. Yerer, K. Sak, et al., Role of reactive oxygen species in cancer progression: molecular mechanisms and recent advancements, Biomolecules 9 (2019).

[14] D. Zhang, Z. Luo, Y. Jin, Y. Chen, T. Yang, Q. Yang, et al., Azelaic acid exerts antileukemia effects against acute myeloid leukemia by regulating the prdxs/ROS signaling pathway, Oxid Med Cell Longev 2020 (2020) 1295984.

[15] F.L. Zhou, Q. Shen, F.X. Claret, Novel roles of reactive oxygen species in the pathogenesis of acute myeloid leukemia, J. Leukoc. Biol. 94 (2013) 423–429.

[16] P.D. Liu, M. Begley, W. Michowski, H. Inuzuka, M. Ginzberg, D.M. Gao, et al., Cell-cycle-regulated activation of Akt kinase by phosphorylation at its carboxyl terminus, Nature 508 (2014) 541.

[17] C. Park, H.J. Cha, H. Lee, H. Hwang-Bo, S.Y. Ji, M.Y. Kim, et al., Induction of G2/M cell cycle arrest and apoptosis by genistein in human bladder cancer T24 cells through inhibition of the ROS-dependent PI3k/akt signal transduction pathway, Antioxidants-Basel 8 (2019).

[18] G.Y. Liou, P. Storz, Reactive oxygen species in cancer, Free Radic. Res. 44 (2010) 479–496.

[19] Y.B. Feng, X.X. Hua, R.W. Niu, Y. Du, C.J. Shi, R.P. Zhou, et al., ROS play an important role in ATPR inducing differentiation and inhibiting proliferation of leukemia cells by regulating the PTEN/PI3K/AKT signaling pathway, Biol. Res. 52 (2019).

[20] S.Y. Wu, Y.C. Wen, C.C. Ku, Y.C. Yang, J.M. Chow, S.F. Yang, et al., Penfluridol triggers cytoprotective autophagy and cellular apoptosis through ROS induction and activation of the PP2A-modulated MAPK pathway in acute myeloid leukemia with different FLT3 statuses, J. Biomed. Sci. 26 (2019).

[21] H. Pelicano, D. Carney, P. Huang, ROS stress in cancer cells and therapeutic implications, Drug Resist. Updates : reviews and commentaries in antimicrobial and anticancer chemotherapy 7 (2004) 97–110.

[22] J.R. Sillar, Z.P. Germon, G.N. DeIuliis, M.D. Dun, The role of reactive oxygen species in acute myeloid leukaemia, Int. J. Mol. Sci. 20 (2019).

[23] D. Trachootham, J. Alexandre, P. Huang, Targeting cancer cells by ROS-mediated mechanisms: a radical therapeutic approach? Nat. Rev. Drug Discov. 8 (2009) 579–591.

[24] B.W. Yang, Y. Chen, J.L. Shi, Reactive oxygen species (ROS)-Based nanomedicine, Chem. Rev. 119 (2019) 4881–4985.

[25] L. Cai, C. Lin, N. Yang, Z. Huang, S. Miao, X. Chen, et al., Preparation and characterization of nanoparticles made from Co-incubation of SOD and glucose, Nanomaterials 7 (2017).

[26] C. Korsvik, S. Patil, S. Seal, W.T. Self, Superoxide dismutase mimetic properties exhibited by vacancy engineered ceria nanoparticles, Chem. Commun. (2007) 1056–1058.

[27] I. Celardo, J.Z. Pedersen, E. Traversa, L. Ghibelli, Pharmacological potential of cerium oxide nanoparticles, Nanoscale 3 (2011) 1411–1420.

[28] T. Pirmohamed, J.M. Dowding, S. Singh, B. Wasserman, E. Heckert, A.S. Karakoti, et al., Nanoceria exhibit redox state-dependent catalase mimetic activity, Chem. Commun. 46 (2010) 2736–2738.

[29] Y.H. Lin, J.S. Ren, X.G. Qu, Nano-gold as artificial enzymes: hidden talents, Adv. Mater. 26 (2014) 4200–4217.

[30] B.X. Li, T. Gu, T. Ming, J.X. Wang, P. Wang, J.F. Wang, et al., (Gold core)@(ceria shell) nanostructures for plasmon-enhanced catalytic reactions under visible light, ACS Nano 8 (2014) 8152–8162.

[31] L. Ye, X.P. Duan, S. Wu, T.S. Wu, Y.X. Zhao, A.W. Robertson, et al., Self-regeneration of Au/CeO2 based catalysts with enhanced activity and ultra-stability for acetylene hydrochlorination, Nat. Commun. 10 (2019).

[32] H.L. Jia, A.X. Du, H. Zhang, J.H. Yang, R.B. Jiang, J.F. Wang, et al., Site-Selective growth of crystalline ceria with oxygen vacancies on gold nanocrystals for near-infrared nitrogen photofixation, J. Am. Chem. Soc. 141 (2019) 5083–5086.

[33] S. Bhagat, N.V.S. Vallabani, V. Shutthanandan, M. Bowden, A.S. Karakoti, S. Singh, Gold core/ceria shell-based redox active nanozyme mimicking the biological multienzyme complex phenomenon, J. Colloid Interface Sci. 513 (2018) 831–842.

[34] M. Farell, A. Self, C. Guza, H. Song, L. Apollon, E.W. Gomez, et al., Lipid-functionalized graphene loaded with hMnSOD for selective inhibition of cancer cells, ACS Appl. Mater. Interfaces 12 (2020) 12407–12416.

[35] L.Z. Gao, J. Zhuang, L. Nie, J.B. Zhang, Y. Zhang, N. Gu, et al., Intrinsic peroxidase-like activity of ferromagnetic nanoparticles, Nat. Nanotechnol. 2 (2007) 577–583.

[36] Z.W. Chen, J.J. Yin, Y.T. Zhou, Y. Zhang, L. Song, M.J. Song, et al., Dual enzyme-like activities of iron oxide nanoparticles and their implication for diminishing cytotoxicity, ACS Nano 6 (2012) 4001–4012.

[37] E.G. Heckert, A.S. Karakoti, S. Seal, W.T. Self, The role of cerium redox state in the SOD mimetic activity of nanoceria, Biomaterials 29 (2008) 2705–2709.

[38] S.S. Lee, W.S. Song, M.J. Cho, H.L. Puppala, P. Nguyen, H.G. Zhu, et al., Antioxidant properties of cerium oxide nanocrystals as a function of nanocrystal diameter and surface coating, ACS Nano 7 (2013) 9693–9703.

[39] T.M. Weiger, A. Hermann, Cell proliferation, potassium channels, polyamines and their interactions: a mini review, Amino Acids 46 (2014) 681–688.

[40] A. Blazquez-Castro, E. Carrasco, M.I. Calvo, P. Jaen, J.C. Stockert, A. Juarranz, et al., Protoporphyrin IX-dependent photodynamic production of endogenous ROS stimulates cell proliferation, Eur. J. Cell Biol. 91 (2012) 216–223.

[41] J.C. Patterson, B.A. Joughin, B. van de Kooij, D.C. Lim, D.A. Lauffenburger, M.B. Yaffe, ROS and oxidative stress are elevated in mitosis during asynchronous cell cycle progression and are exacerbated by mitotic arrest, Cell Syst 8 (2019) 163. -+.

[42] Y. Qin, X. Pan, T.T. Tang, L. Zhou, X.G. Gong, Anti-proliferative effects of the novel squamosamide derivative (FLZ) on HepG2 human hepatoma cells by regulating the cell cycle-related proteins are associated with decreased Ca(2+)/ROS levels, Chem. Biol. Interact. 193 (2011) 246–253.

[43] H.P. Wang, S.Y. Qian, F.Q. Schafer, F.E. Domann, L.W. Oberley, G.R. Buettner, Phospholipid hydroperoxide glutathione peroxidase protects against singlet oxygen-induced cell damage of photodynamic therapy, Free Radical Biol. Med. 30 (2001) 825–835.

[44] Q.R. Ding, T. Jin, Z.Z. Wang, Y. Chen, Catalase potentiates retinoic acid-induced THP-1 monocyte differentiation into macrophage through inhibition of peroxisome proliferator-activated receptor gamma, J. Leukoc. Biol. 81 (2007) 1568–1576.

[45] P. Tsvetkov, A. Detappe, K. Cai, H.R. Keys, Z. Brune, W. Ying, et al., Mitochondrial metabolism promotes adaptation to proteotoxic stress, Nat. Chem. Biol. 15 (2019) 681–689.

[46] P. Ma, H. Xiao, C. Yu, J. Liu, Z. Cheng, H. Song, et al., Enhanced Cisplatin chemotherapy by iron oxide nanocarrier-mediated generation of highly toxic reactive oxygen species, Nano Lett. 17 (2017) 928–937.

[47] Q. Cui, J.Q. Wang, Y.G. Assaraf, L. Ren, P. Gupta, L. Wei, et al., Modulating ROS to overcome multidrug resistance in cancer, Drug Resist. Updates : reviews and commentaries in antimicrobial and anticancer chemotherapy 41 (2018) 1–25.

[48] V. Trujillo-Alonso, E.C. Pratt, H. Zong, A. Lara-Martinez, C. Kaittanis, M.O. Rabie, et al., FDA-approved ferumoxytol displays anti-leukaemia efficacy against cells with low ferroportin levels, Nat. Nanotechnol. (2019) 616–622.

[49] C. Zhao, J. Chen, R. Zhong, D.S. Chen, J. Shi, J. Song, Oxidative species-selective materials for diagnostic and therapeutic applications, Angew. Chem. (2020) 9804–9827.

[50] Y. Chen, N. Li, J. Wang, X. Zhang, W. Pan, L. Yu, et al., Enhancement of mitochondrial ROS accumulation and radiotherapeutic efficacy using a Gd-doped titania nanosensitizer, Theranostics 9 (2019) 167–178.

[51] P. Lee, N.S. Chandel, M.C. Simon, Cellular adaptation to hypoxia through hypoxia inducible factors and beyond, Nat. Rev. Mol. Cell Biol. (2020) 268–283.

[52] S. Saikolappan, B. Kumar, G. Shishodia, S. Koul, H.K. Koul, Reactive oxygen species and cancer: a complex interaction, Canc. Lett. 452 (2019) 132–143.

[53] J. Chen, H. Luo, Y. Liu, W. Zhang, H. Li, T. Luo, et al., Oxygen-self-produced nanoplatform for relieving hypoxia and breaking resistance to sonodynamic treatment of pancreatic cancer, ACS Nano 11 (2017) 12849–12862.

[54] T. Montini, M. Melchionna, M. Monai, P. Fornasiero, Fundamentals and catalytic applications of CeO2-based materials, Chem. Rev. 116 (2016) 5987–6041.